1st International Seminar on Dam Protection against Overtopping and Accidental Leakage
M.Á. Toledo, R. Morán, E. Oñate (Eds)
Madrid, 24-25 November 2014

CHARACTERIZATION OF THE DYNAMIC ACTIONS AND SCOUR ESTIMATION DOWNSTREAM OF A DAM

LUIS G. CASTILLO[1] AND JOSE M. CARRILLO[1]

[1]Universidad Politécnica de Cartagena (UPCT)
Paseo Alfonso XIII, 52
30203 Cartagena, Spain
e-mail: luis.castillo@upct.es - jose.carrillo@upct.es
Key words: Dam, Spillway, Scour, Pressure fluctuations, Erodibility index, CFD.

Summary. The study analyzes the expected changes in the Paute River, located in Ecuador, as a result of the construction of the Paute-Cardenillo Dam (owned by Celec Ep-Hidropaute). The dam will integrate the National Electric System of Ecuador with a total electricity installed capacity of 600 MW which will produce 13000 GWh per year. To evaluate the stability and safety of the structure, it is necessary to ascertain the shape and dimensions of the scour generated downstream from the dam. The scour, due to the operation of the spillway and outlets, is studied with three complementary procedures: empirical formulae obtained in models and prototypes, semi-empirical methodology based on pressure fluctuations-erodibility index and computational fluid dynamics simulations.

1 DAM CHARACTERISTICS

The Paute-Cardenillo Dam, located in Ecuador, is a double curvature arch dam with a maximum height of 135 m to the foundations. The top level is located at 926 meters above mean sea level (MASL). The reservoir has a length of 2.98 km with normal maximum water level located at 924 MASL. The river bed consists of a layer of 24 m of alluvial, below which there is a layer of 10 m of weathered rock. It has a free surface weir controlled by sluices that spill a flow of Q_4 = 700 m^3/s (return period TR = 4 years) and a half-height outlet with two almost symmetrical ducts. Considering the maximum normal operating level (924 MASL), the intermediate outlet capacity is Q_{40} = 1760 m^3/s. Hence, the total flow of the weir and half-height outlet is Q_{100} = 2340 m^3/s. If the bottom outlet were considered, the discharge capacity of the dam would be Q_{10000} = 5520 m^3/s.

2 EMPIRICAL FORMULAE

In the study, 29 formulae are examined. The scour hole is estimated for different return periods flows.

Most of the equations were obtained by dimensional and statistic analysis of data obtained in Froude scale reduced models, with few formulae based on prototypes and many obtained for the ski-jump. As discharge is produced by a free surface weir and in pressure conditions by an intermediate outlet, the general expression is modified which provides the following

simplified general expression:

$$D_s = h + D = K\frac{q^x H_n^y h^w}{g^v d^z} \quad (1)$$

where D_s is the scour depth below tailwater level, h the tailwater depth, D the scour depth below the original bed, K an experimental coefficient, q the specific flow, H_n the energy net head, and d the characteristic size of bed material. The meaning of the rest variables can be seen in Figure 1.

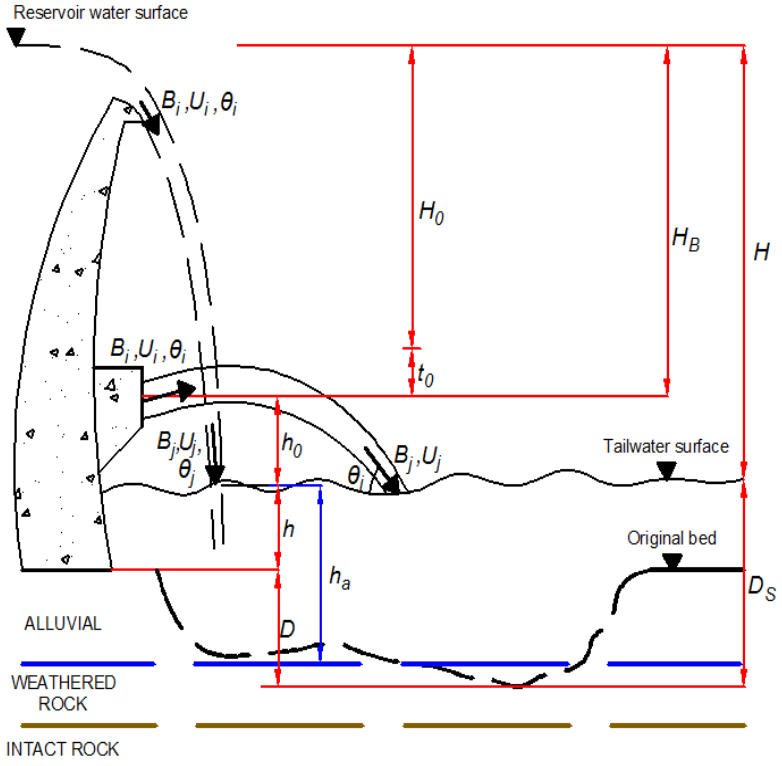

x, y, w, v , z. Empirical exponents defined by regression or optimization.

t_0 = energy losses in the duct.

$H_n = H_0 = H_B - t_0$. Net energy head at the exit of the outlet.

$H_n = H$. Falling height from reservoir level to tailwater level (ski-jump and free surface weir).

h_0. Vertical distance between outlet exit and tailwater level.

h_a. Vertical distance between tailwater level and scour bed.

B_i, U_i, θ_i. Thickness, velocity and angle of the jet in initial conditions.

B_j, U_j, θ_j. Total thickness, velocity and angle of the jet in impingement conditions.

Figure 1: Scheme of scour in Paute-Cardenillo Dam

Table 1 shows the coefficients corresponding to five simplified formulae with values that fall in the mean values +/- 1 standard deviation, while Table 2 shows five more general expressions with values in the same range.

Figure 2 shows the results obtained for the free surface weir. The mean value +/- 1 standard deviation is indicated. If the mean value for the design flow (700 m^3/s) were considered, the scour could reach a depth of 15 m. However, if the mean value + 1 standard deviation were taken into account, then the flow of 500 m^3/s would penetrate the weathered rock (scour about 30 m).

Table 1: Coefficients of five scour simplified formulae with values that fall in the mean value +/- 1 standard deviation

Author	*K*	*x*	*y*	*z*	*d*
Hartung [25]	1.400	0.64	0.360	0.32	d_{85}
Chee and Padiyar [17]	2.126	0.67	0.180	0.063	d_m
Bisaz and Tschopp [3]	2.760	0.50	0.250	1.00	d_{90}
Martins-A [29]	1.500	0.60	0.100	0.00	-
Machado [28]	1.350	0.50	0.3145	0.0645	d_{90}

Table 2: Five scour general formulae with values that fall in the mean value +/- 1 standard deviation

AUTHOR (YEAR)	**FORMULAE**
Jaeger [27]	$D_S = 0.6q^{0.5}H_n^{0.25}(h/d_m)^{0.333}$
Rubinstein [36]	$D_S = h + 0.19\left(\frac{H_n + h}{d_{90}}\right)^{0.75}\left(\frac{q^{1.20}}{H_n^{0.47}h^{0.33}}\right)$
Mirskhulava [34]	$D_S = \left(\frac{0.97}{\sqrt{d_{90}}} - \frac{1.35}{\sqrt{H_n}}\right)\frac{q \cdot sin\theta_T}{1 - 0.175 \cdot cot\theta_T} + 0.25h$
Mason-B [30]	$D_S = 3.39\frac{q^{0.60}(1+\beta)^{0.30}h^{0.16}}{g^{0.30}d^{0.06}}$
Bombardelli and Gioia [6]	$D_S = K\frac{q^{0.67}H_n^{0.67}h^{0.15}}{g^{0.33}d^{0.33}}\left(\frac{\rho}{\rho_s - \rho}\right)$

d_m. Average particle size of the bed material.
d_{90}. Bed material size in which 90% is smaller in weight.
θ_T. Impingement jet angle.
g (9.81 m/s^2). Gravity.
β. Air-water relationship.
ρ. Water density.
ρ_s. Density of sediment.

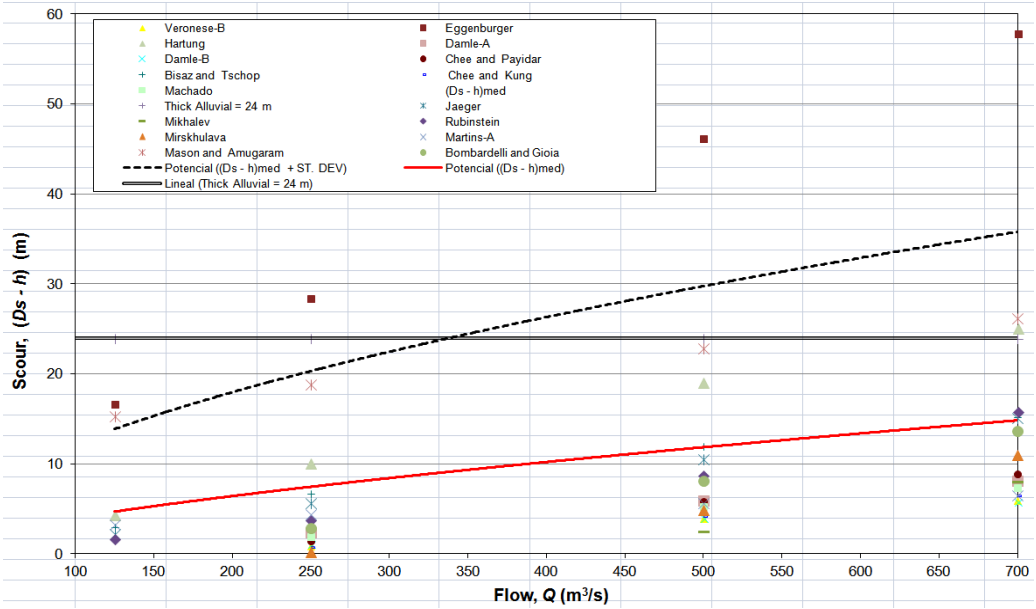

Figure 2: Scour of alluvial and weathered rock for the free surface weir

Figure 3 shows the results obtained for the half-height outlet. The mean value +/- 1 standard deviation is indicated. The jet would scour the alluvial layer (24 m) with a return period flow Q_{22} = 1320 m^3/s. The design flow (Q_{40} = 1760 m^3/s) would not reach the intact rock. However, if the mean value + 1 standard deviation were taken into account, then the flow of 1250 m^3/s would erode the weathered rock layer (scour about 34 m).

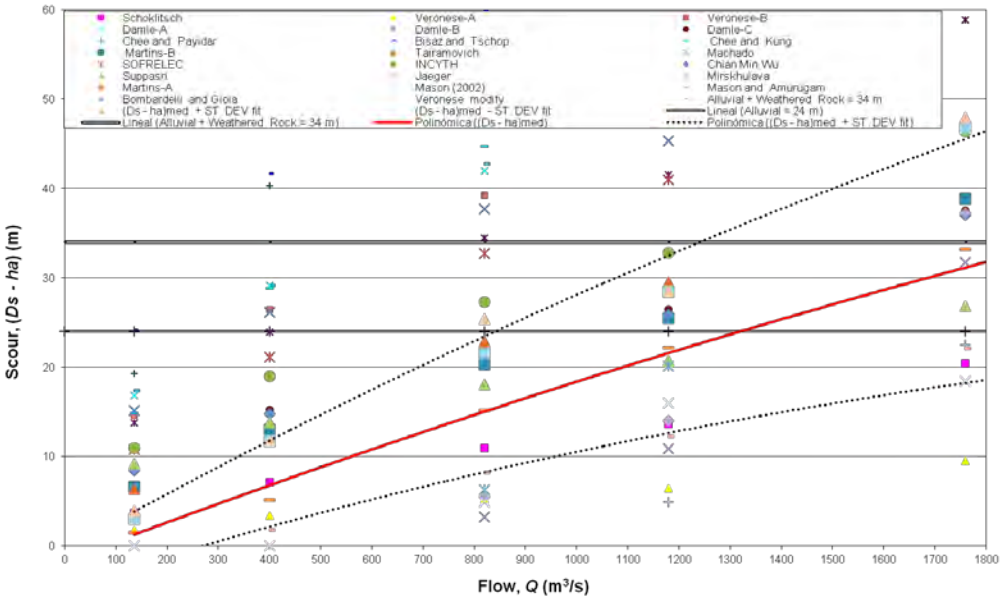

Figure 3: Scour of alluvial and weathered rock for the half-height outlet

3 SEMI-EMPIRICAL METHODOLOGY

The erodibility index is based on an erosive threshold that relates the magnitude of relative erosion capacity of water and the relative capacity of a material (natural or artificial) to resisting scour. There is a correlation between the stream power or magnitude of the erosive capacity of water (P) and a mathematical function [$f(K)$] that represents the relative capacity of the material to resisting erosion. On the erosion threshold, this may be expressed by the relationship $P = f(K)$. If $P > f(K)$, the erosion threshold is being exceeded and the material is eroded.

Scour in turbulent flow is not a shear process. It is caused by turbulent, fluctuating pressures (Annandale [2]). Quantification of pressure fluctuations of incident jets in stilling basins has been studied mainly by Ervine and Falvey [20], Ervine et al. [21], Castillo [9, 11, 12, 14], Castillo et al. [10, 13], Puertas [35], Bollaert [4], Bollaert and Schleiss [5], Melo et al. [33], Felderspiel [22], and Carrillo [8].

The dynamic pressures of jets are a function of the turbulence intensity at the discharge conditions, length of the jet flight, diameter (circular jet) or thickness (rectangular jet) in impingement jet conditions and water cushion depth. Annandale [1, 2] summarized and established a relationship between the stream power and the erodibility index for a wide

variety of materials and flow conditions. The stream power per unit of area available of an impingement jet is:

$$P_{jet} = \frac{\gamma Q H}{A} \tag{2}$$

where γ is the specific weight of water, Q the flow, H the drop height or the upstream energy head, and A the jet area on the impact surface. The erodibility index is defined as:

$$K = M_s \cdot K_b . K_d \cdot J_s \tag{3}$$

where M_s is the number of resistance of the mass, K_b the number of the block size, K_d the number of resistance to shear strength on the discontinuity contour, and J_s the number of structure relative of the grain. Table 3 shows the formulae of the parameters.

Table 3: Erodibility index parameters (Adapted from Annandale [2])

Material	Formulae	Parameters
Rock	$M_s = 0.78 C_r UCS^{1.05}$ $when$ $UCS \leq 10\ MPa$ $M_s = C_r UCS$ $when$ $UCS > 10\ MPa$ $C_r = \frac{g\rho_r}{\gamma_r}$	C_r. Relative density ratio. ρ_r. Rock density. g (9.81 m/s^2). Gravity. γ_r ($27 \cdot 10^3$ N/m^3). Specific weight of the intact rock.
Non-cohesive granular	The relative magnitude is obtained from the *SPT* results. When this value exceeds 80, the non-cohesive granular material is considered equivalent to rock.	
Rock	$K_b = \frac{RQD}{J_n}$	*RQD* values are between 5 and 100, J_n between 1 and 5, and K_b between 1 and 100.
Non-cohesive granular	$K_b = 1000 D^3$	*D*. Diameter of the average block.
Rock	$K_d = \frac{J_r}{J_a}$	
Non-cohesive granular	$K_d = tan\phi$	Φ. Angle of residual or internal friction of the granular material.

The threshold of rock strength to the stream power, expressed in kW/m^2, is calculated and based on the erodibility index K:

$$\begin{aligned} P_{rock} &= 0.48 K^{0.44} \quad if \quad K \leq 0.1 \\ P_{rock} &= K^{0.75} \quad if \quad K > 0.1 \end{aligned} \tag{4}$$

The dynamic pressure in the bottom of the stilling basin is based on two components: the mean dynamic pressure (C_p) and the fluctuating dynamic pressure (C_p'). These dynamic pressure coefficients are used as estimators of the stream power reduction coefficients, by an effect of the jet disintegration in the air and their diffusion in the stilling basin.

Hence, the dynamic pressures are also a function of the fall height to disintegration height ratio (H/L_b) and water cushion to impingement jet thickness (Y/B_j). Thus, the total dynamic pressure is expressed as:

$$P_{total} = C_p(Y/B_j)P_{jet} + FC_p'(Y/B_j)P_{jet} \quad (5)$$

where $C_p(Y/B_j)$ is the mean dynamic pressure coefficient, $C_p'(Y/B_j)$ the fluctuating dynamic pressure coefficient, P_{jet} the stream power per unit of area, and F the reduction factor of the fluctuating dynamic pressure coefficient. In rectangular jet case (nappe flow), Castillo and Carrillo [16] and Carrillo [8] adjusted the formulae by using new laboratory data (Figures 4, 5 and 6).

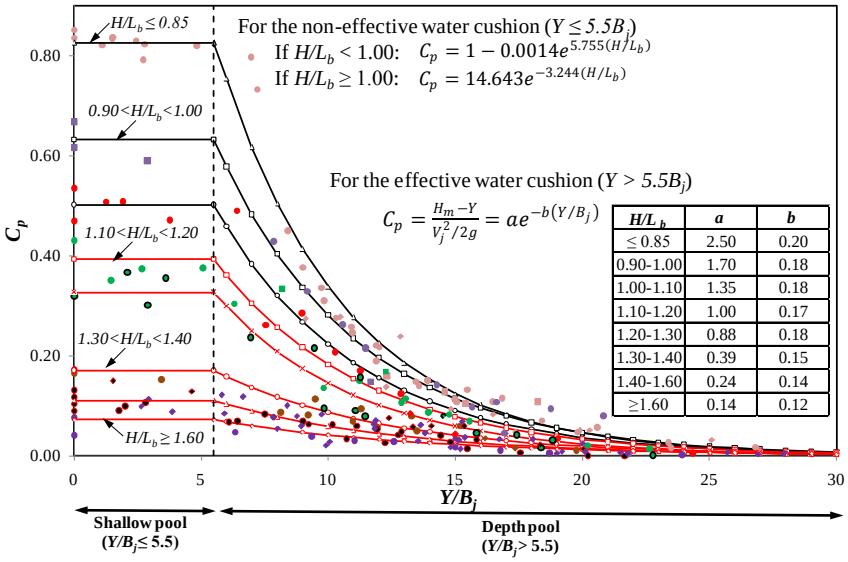

H/L_b	a	b
≤ 0.85	2.50	0.20
0.90-1.00	1.70	0.18
1.00-1.10	1.35	0.18
1.10-1.20	1.00	0.17
1.20-1.30	0.88	0.18
1.30-1.40	0.39	0.15
1.40-1.60	0.24	0.14
≥1.60	0.14	0.12

Figure 4: Mean dynamic pressure coefficient, C_p, for the nappe flow case

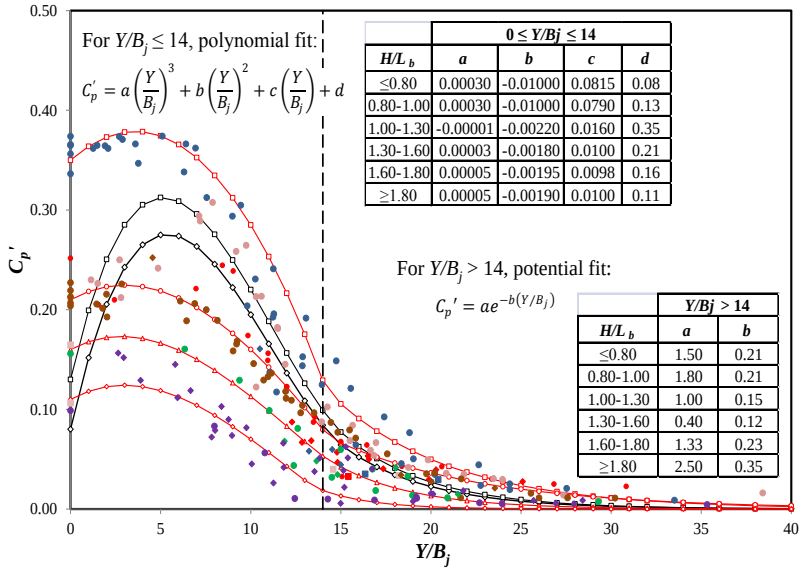

	0 ≤ Y/Bj ≤ 14			
H/L_b	a	b	c	d
≤0.80	0.00030	-0.01000	0.0815	0.08
0.80-1.00	0.00030	-0.01000	0.0790	0.13
1.00-1.30	-0.00001	-0.00220	0.0160	0.35
1.30-1.60	0.00003	-0.00180	0.0100	0.21
1.60-1.80	0.00005	-0.00195	0.0098	0.16
≥1.80	0.00005	-0.00190	0.0100	0.11

	Y/Bj > 14	
H/L_b	a	b
≤0.80	1.50	0.21
0.80-1.00	1.80	0.21
1.00-1.30	1.00	0.15
1.30-1.60	0.40	0.12
1.60-1.80	1.33	0.23
≥1.80	2.50	0.35

Figure 5: Fluctuant dynamic pressure coefficient, C_p', for the nappe flow case

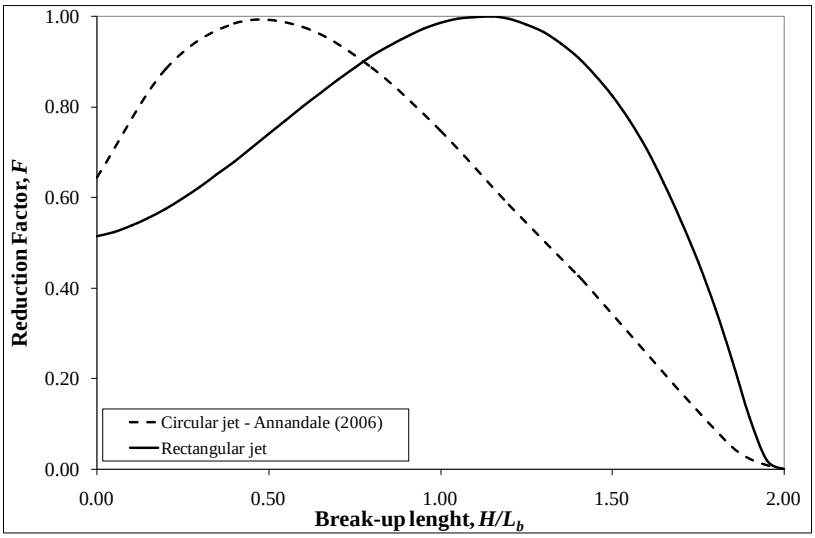

Figure 6: Reduction factor *F* of fluctuating dynamic pressure coefficient

Table 4 shows the values of the different variables considered and their respective calculus in the semi-empirical methodology.

Table 4: Semi-empirical methodology. Input and calculated values

Angle of rock friction, *SPT* (º)	38	Number of join system (calculated), J_n	1.83
Specific weight (KN/m^3)	27.64	Discontinuity spacing, J_x, J_y, J_z (m)	0.50
Unconfined compress. resistant, *UCS* (Mpa)	50	Average block diameter (calculated), (m)	0.50
Relative density coefficient, *Cr*	1.02	Roughness degree, J_r	2.00
RQD (calculated)	82.66	Alteration degree, J_a	1.00

Table 5 shows the results obtained in the three types of material existent in the place of the dam and the concrete slab proposed. In Figure 7 the stream power of the free surface weir jet is indicated, together with the power threshold of alluvial, weathered and intact rock.

Table 5: Stream power of free surface jets for different flows as a function of the erodibility: alluvial, weathered rock, intact rock and concrete slab indexes (water cushion depth 24 m)

	Alluvial	**Weathered rock**	**Intact rock**	**Concrete**
M_s	0.19	0.41	51.19	20.47
K_b	11.39	125	49.18	49.18
K_d	0.78	0.78	2.00	5.33
J_s	1.00	1.00	0.60	1.00
Erodibility index, *K*	1.69	40.04	3021	7280
Stream power, P_{rock} (kw/m^2)	1.50	16	408	788

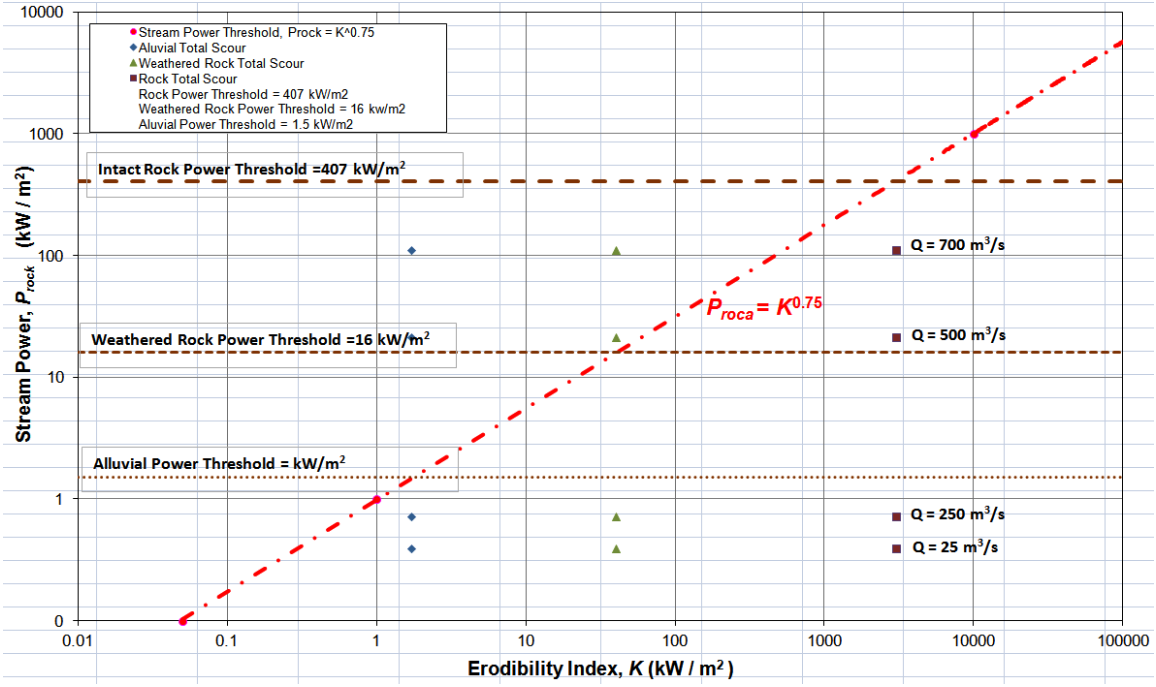

Figure 7: Free surface weir. Stream power of the jet for different flows as a function of the erodibility: alluvial, weathered rock and intact rock indexes (water cushion depth 24 m)

Considering a water cushion depth of 24 m, the flow rate of 500 m^3/s would have the power to erode weathered rock, although the design flow of 700 m^3/s would not have enough power to erode the intact rock. These results confirm that the maximum scour of the free surface weir could be near to 34 m.

We can observe that the half-height outlet case does not correspond strictly with circular neither rectangular (nappe flow) jet case. For circular jets, the C_p and C_p' are valid for $H/L_b \leq 0.50$ (Ervine et al., [21]). However, for the design flow (Q_{40} = 1760 m^3/s) the H/L_b = 1.67. For this reason the calculus were carried out by using the rectangular analogy.

The stream power threshold of weathered rock ($P_{weathered\_rock}$ = 16 kW/m^2) does not resist the flow of annual return period (Q_{ma} = 136 m^3/s). The intact rock stream power (P_{rock} = 408 kW/m^2) could resist up to a flow return period of 5 years (Q_5 = 820 m^3/s). The Q_{10} = 1180 m^3/s would exceed the rock strength.

As a solution to the scour, a concrete slab of 20 MPa characteristic strength and thickness of 2 m (P_{conc} = 788 kW/m^2) is placed directly on the alluvial level (796 MASL). The geometry of the pre-excavated basin should be similar to the geometry of the basin that would be formed with the flow Q_{40} = 1760 m^3/s. Figure 8 indicates that the concrete slab would resist the power stream of the design flow (P_{jet} = 664.95 kW/m^2).

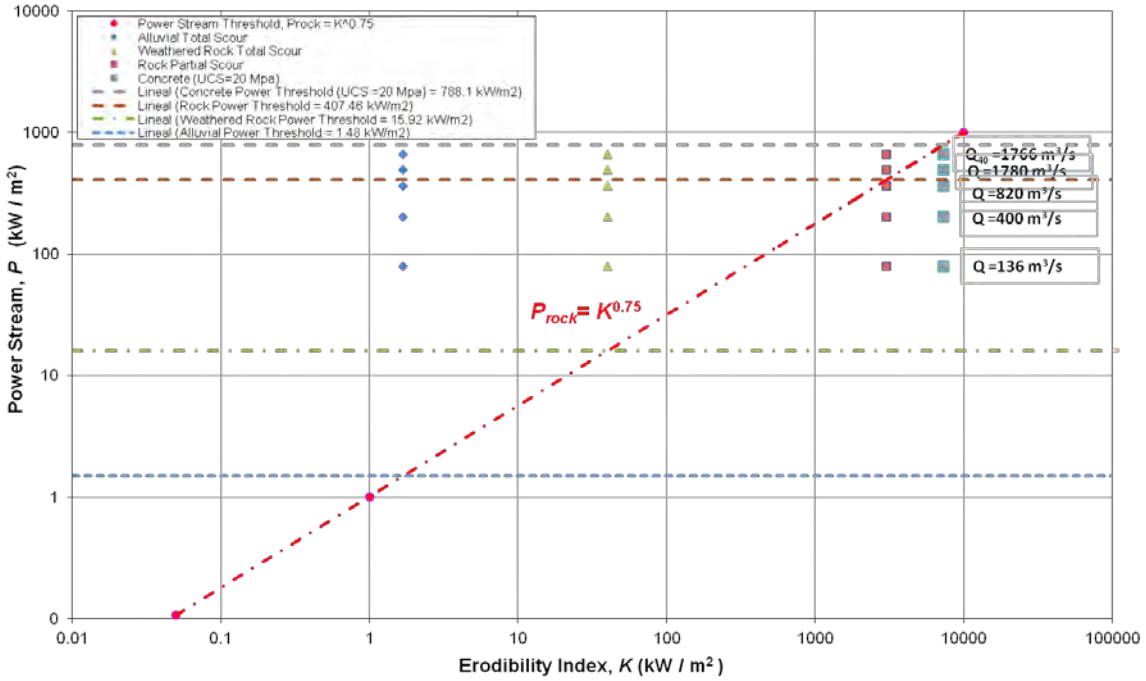

Figure 8: Half-height outlet. Stream power of the jet for different flows as a function of the erodibility: alluvial, weathered rock, intact rock and concrete cases (Water cushion depth 24 m)

4 NUMERICAL SIMULATION

As a complement of the empirical and semi-empirical methodologies, three-dimensional mathematical model simulations were carried out. These programs allow a more detailed characterization than one-dimensional and two-dimensional numerical models and, thus, a detailed study of local effects of the sediments transport. The numerical simulation of the hydraulic behavior and scour by the action of the free surface weir, intermediate and bottom outlets were also analyzed.

The computational fluid dynamics (CFD) program FLOW-3D was used. This program solves the Navier-Stokes equations discretized by finite differences. It incorporates various turbulence models, a sediment transport model and an empirical model bed erosion (Guo [24]; Mastbergen and Von den Berg [32]; Brethour and Burnham [7]), together with a method for calculating the free surface of the fluid without solving the air component (Hirt and Nichols [26]). Pressures obtained in the stagnation point and their associated mean dynamic pressure coefficients were compared with the parametric methodology proposed by Castillo [12, 14], actualized by Castillo and Carrillo [16] and Carrillo [8].

In order to simulate the proper functioning of the free surface weir, several simulations were carried out by means of sensibility analysis: air entrainment models, turbulence models, grid size and type of solver, among others (Figure 9).

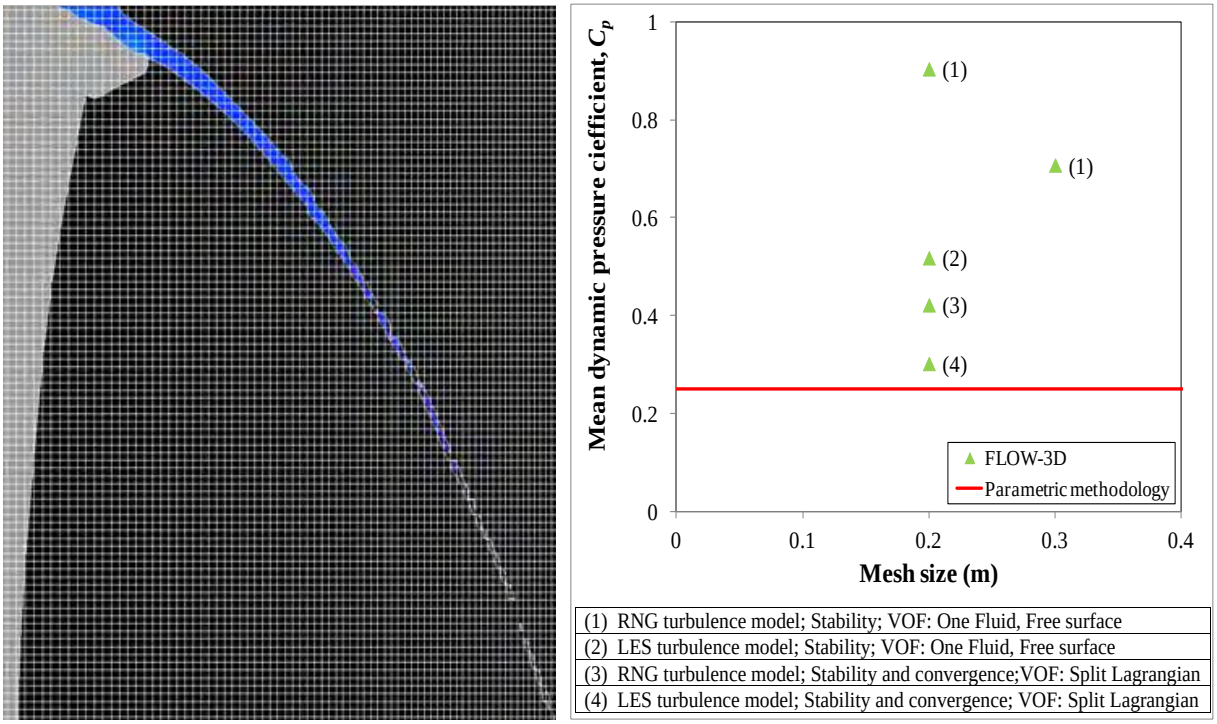

Figure 9: Mesh and sensibility analysis of FLOW-3D

We can observe that the results are anomalous when RNG *k-ε* turbulence model and the one fluid free surface method are used. So, if the mesh size is reduced from 0.30 m to 0.20 m, C_p changes from 0.71 to 0.90. However, when the RNG *k-ε* model is used with the split Lagrangian free surface method, then the results are more similar to the expected value.

The most accurate results were obtained by using a mesh size of 0.2 m, and large eddy simulation (LES) turbulence model. In the solver options, the stability and convergence method was selected and the free surface solved with the split Lagrangian method.

Table 6 compares the mean pressure and the mean dynamic pressure coefficient obtained by the non-effective water cushion case. Results were similar to the parametric methodology. It may be observed that the mean dynamic pressure and C_p coefficient obtained with FLOW-3D are somewhat greater than parametric methodology values, which is due to the air entrainment model not resolving the two-phase flow in an appropriate way.

Table 6: Comparison of pressures and C_p, considering a water cushion depth of 2 m

	Parametric methodology	**FLOW-3D**
Drop height (m)	102.0	102.0
Mean dynamic pressure (m)	30.56	33.44
Mean dynamic pressure coefficient, C_p	0.28	0.31

As far as scour is concerned, free surface weir jets tended to impact on a small area. The upstream face of the scour bowl occurred approximately 29 m downstream from the dam. The plant scour was near 24 m long and 53 m wide (Figure 10). Erosion generated a scour depth of 22 m, which was a little greater than that calculated with the mean value of the empirical formulae and similar to that obtained with semi-empirical methodology.

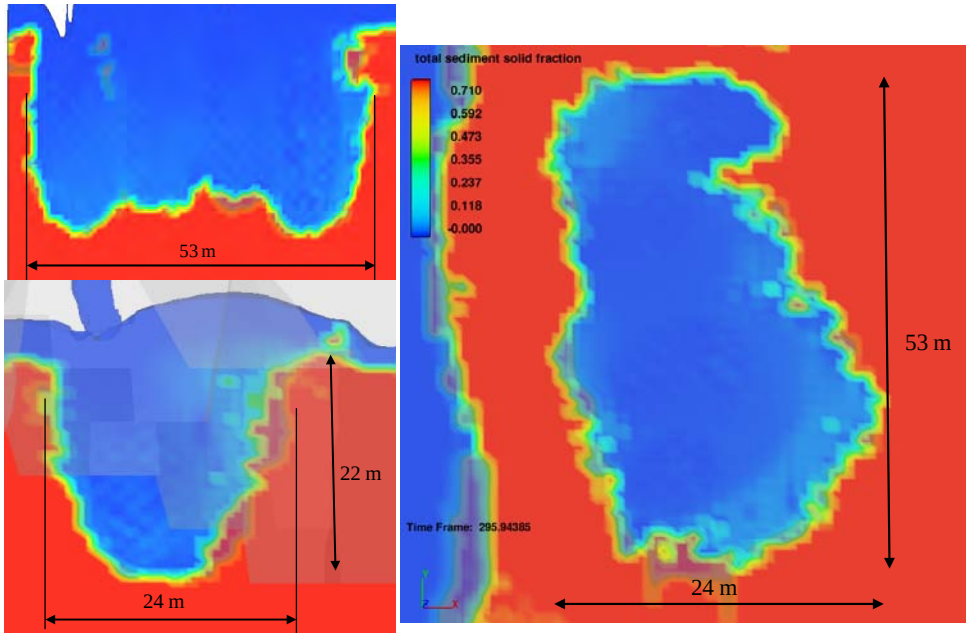

Figure 10: Front, lateral, and top view of the scour due to the free surface weir

For the simulation of half-height outlet ducts (5.00 x 5.80 m), the selection of the mesh size is function of their dimensions and of the thickness of the falling jets. The mesh consisted in hexahedral elements of 1 m. The Re-Normalization Group (RNG) k-ε turbulence model was selected. The volume-of-fluid advection was solved with the Split Lagrangian method. The time-step size was controlled by stability and convergence criteria.

Pressures obtained in the stagnation point and their associated mean dynamic pressure coefficients were compared with the parametric methodology [12, 14, 16, 8].

As far as the numerical simulation is concerned, the scour shape considering the concrete slab was analyzed. In this way, the level 798 m was considered as a non erodible. For the design flow, the half-height outlet jets tend to impact on a small area.

The upstream face of the scour occurred approximately 85 m downstream from the dam. The plant scour was near 108 m long and 50 m wide (Figure 11). Scour would reach the left natural slope and could cause landslides. The pre-excavated stilling basin shape should be adjusted to the geometry and the space available. Figure 12 shows the velocities vectors in lateral and top views of the pre-excavated basin.

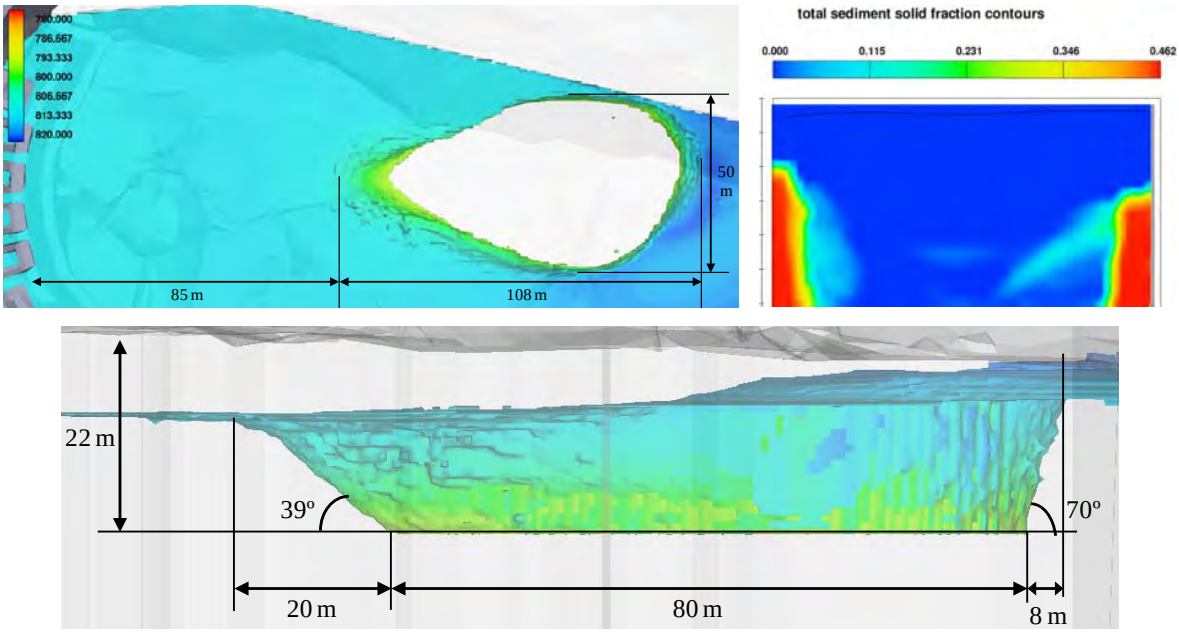

Figure 11: Top, front and lateral views of the scour due to the half-height outlet

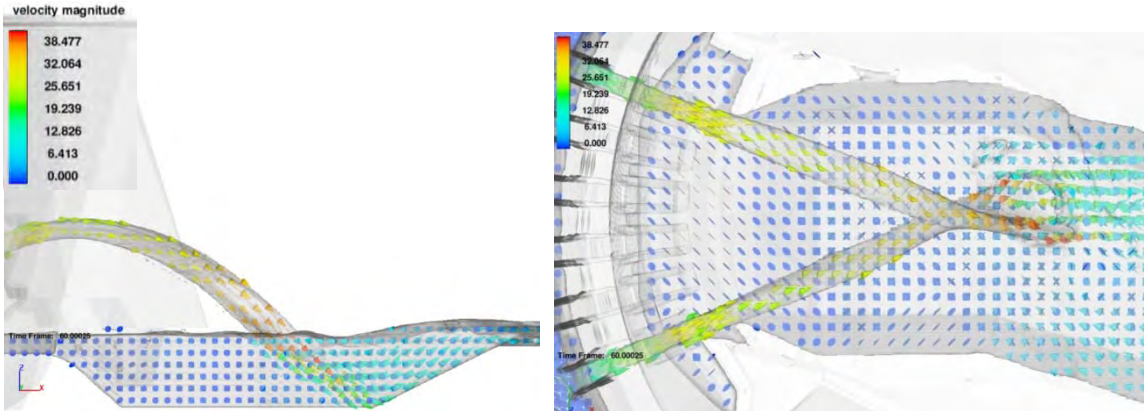

Figure 12: Lateral and top views of the velocity vectors in the pre-excavated stilling basin

5 CONCLUSION

In this paper, similar results have been obtained by solving the problem from three different perspectives: empirical formulations, erosion potential semi-empirical formulation and CFD simulations.

The results demonstrate the suitability of crossing methodologies to solve complex phenomena. Thus, numerical simulations were used to complement the classical formulations, allowing a better understanding of the physical phenomena in order to obtain an adequate solution. Methodology leads us to propose a pre-excavated stilling basin.

The basin would allow to generate an effective water cushion. Besides this, it would reduce the sedimentation due to the excavation and the material transported by the river, especially during the flushing operations of the reservoir. The pre-excavated basin also would help to have a symmetric and regular flow, reducing the risk of potential landslides.

ACKNOWLEDGMENTS

The authors are grateful to CELEC EP - Hidropaute and the Consorcio POYRY-Caminosca Asociados for the data provided.

REFERENCES

[1] G.W. Annandale, Erodibility. *Journal of Hydraulic Research*, 33 (4), 471-494 (1995).
[2] G.W. Annandale, *Scour Technology. Mechanics and Engineering Practice*. McGraw-Hill, (2006).
[3] E. Bisaz and J. Tschopp, Profundidad de erosion al pie de un vertedero para la aplicación de correccion de arroyos en quebradas empinadas. *Proceedings of the Fifth Congreso Latinoamericano de Hidraulica (IAHR)*, Lima, Peru, 447–456, (1972).
[4] E. Bollaert, *Transient Water Pressures in Joint and Formations of Rock Scour due to High-Velocity Jet Impact, Communication Nº. 13*. Laboratory of Hydraulic Constructions, École Polytechnique Fédérale de Lausanne, Switzerland, (2002).
[5] E.F. Bollaert and A. Schleiss, Scour of rock due to the impact of plunging high velocity jets. Part 1: A state-of-the-art review. *Journal of Hydraulic Research*, 41(5), 451-464, (2003).
[6] F.A. Bombardelli and G. Gioia. Scouring of granular beds by jet-driven axisymmetric turbulent cauldrons. *Phys. Fluids*, 18(8), 088-101, (2006).
[7] J. Brethour and J. Burnham, Modeling Sediment Erosion and Deposition with the FLOW-3D Sedimentation & Scour Model. *Flow Science Technical Note, FSI-10-TN85*, 1-22, (2010).
[8] J. M. Carrillo, *Metodología numérica y experimental para el diseño de los cuencos de disipación en el sobrevertido de presas de fábrica*. PhD Thesis. Universidad Politécnica de Cartagena, Spain, (2014).
[9] L. Castillo, *Metodología experimental y numérica para la caracterización del campo de presiones en los disipadores de energía hidráulica. Aplicación al vertido en presas bóveda*. PhD Thesis. Universitat Politécnica de Catalunya, Spain, (1989).
[10] L. Castillo, J. Dolz and J. Polo, Acquisition and analysis of data to characterize dynamic Actions in Hydraulic Energy Dissipators. *XXIV IAHR Congress*. D, 273-280. Madrid, (1991).
[11] L. Castillo, Parametrical Analysis of the Ultimate Scour and Mean Dynamic Pressures at Plunge Pools. *Workshop on Rock Scour due to High Velocity Je*ts. École Polytechnique Fédérale de Lausanne, (2002).
[12] L. Castillo, Areated jets and pressure fluctuation in plunge pools. *The 7th International Conference on Hydroscience and Engineering* (ICHE-2006), IAHR, ASCE, Drexel University. College of Engineering. DSpace Digital Library. DU Haggerty Library,

Philadelphia, USA, (2006).
[13] L. Castillo, J. Puertas and J. Dolz, Discussion about Scour of rock due to the impact of plunging high velocity jets Part I: A state-of-the-art review. *Journal of Hydraulic Research*, 45 (6), 853-858, (2007).
[14] L. Castillo, Pressure characterization of undeveloped and developed jets in shallow and deep pool. *32nd Congress of IAHR*, the International Association of Hydraulic Engineering & Research, Vol. 2, 645-655, Venice, Italy, (2007).
[15] L.G. Castillo and J.M. Carrillo, Hydrodynamics characterization in plunge pool. Simulation with CFD methodology and validation with experimental measurements. *2nd IAHR Europe Congress*, Munich (2012).
[16] L.G. Castillo and J.M. Carrillo, Analysis of the ratio scale in nappe flow case by means of CFD numerical simulations. *Proceedings of 2013 IAHR Congress*, Chengdu, China, (2013).
[17] S.P. Chee and P.V. Padiyar, Erosion at the base of flip buckets. *Enginering Journal, Inst. of Canada*, 52(111), 22-24, (1969).
[18] CONSORCIO PCA. *FASE B: Informe de Factibilidad, Anexo 2, Meteorología, Hidrología y Sedimentología*, (2012).
[19] CONSORCIO PCA. *FASE B: Informe de Factibilidad, Anexo 6, Hidráulica*, (2012).
[20] D.A. Ervine and H.R. Falvey, Behavior of turbulent jets in the atmosphere and plunge pools. *Proceedings of the Institutions of Civil Engineers*, 83 (2), 295-314, (1987).
[21] D.A. Ervine, H.R. Falvey and W. Whiters, Pressure Fluctuations on Plunge Pool Floors. *Journal of Hydraulic Research*, 35 (2), (1997).
[22] M.P. Felderspiel, *Response of an embedded block impacted by high-velocity jets*. PhD Thesis. École Polytechnique Fédérale de Lausanne, Suisse, (2011).
[23] Flow Sciences Incorporated. *FLOW-3D Users Manual Version 10.0*. Santa Fe, New Mexico, (2011).
[24] J. Guo, Hunter Rouse and Shields diagram. *Proc 1th IAHR-APD Congress*, Singapore, 2, 1069-1098, (2002).
[25] W. Hartung, Die Kolkbildung hinter Uberstromen wehren im Hinblick auf eine beweglich Sturzbettgestaltung. *Die Wasser Wirtschaft*, 49(1), 309-313, (1959).
[26] C.W. Hirt and B.D. Nichols, Volume of Fluid (VOF) Method for the Dynamics of Free Boundaries. *Journal of Computational Physics*, 39 (201), (1981).
[27] C. Jaeger, Uber die Aehnlichkeit bei flussaulichen Modellversuchen. *Wasserkraft und Wasserwirtschaft*, 34(23/24), 269, (1939).
[28] L.I. Machado, Formulas to calculate the scour limit on granular or rock beds. *XIII National workshop on large dams*, Subject 1, Rio de Janeiro, Brazil, 35-52, (1980).
[29] R. Martins, Scouring of rocky riverbeds by free-jet spillways. *Water Power & Dam Construction*, April, (1975).
[30] P.J. Mason, Effects of air entrainment on plunge pool scour. *Journal of Hydraulic Engineering*, 115(3), 385-399, (1989).
[31] P.J. Mason and K. Arumugan, Free Jets Scour below Dams and Flip Buckets. *Journal of Hydraulic Engineering, ASCE*, 111(2), 220-235, (1985).
[32] D.R. Mastbergen and J.H. Von den Berg, Breaching in fine sands and the generation of sustained turbidity currents in submarine canyons. *Sedimentology*, 50, 625-637, (2003).
[33] J.F. Melo, A.N. Pinheiro and C.M. Ramos, Forces on plunge pool slabs: influence of

joints location and width. *Journal of Hydraulic Engineering*, 132 (1), 49-60, (2006).
[34] T. E. Mirtskhulava, Alguns Problemas da Erosao nos Leitos dos Rios. Moscow. *Trans. No 443do L.N.E.C.*, (1967).
[35] J. Puertas, *Criterios hidráulicos para el diseño de cuencos de disipación de energía en presas bóveda con vertido libre por coronación*. PhD Thesis, Universidad Politécnica de Cataluña, Spain, (1994).
[36] G.L. Rubinstein, Laboratory investigation of local erosion on channel beds below high overflow dams, *Transactions of Coordination Conferences on Hydraulic Engineering. 1ss. VII, Conference on Hydraulics of High Head Water Discharge Structures*. Gosenergoizdat M.L., (1963).
[37] I.I. Taraimovich, Deformation of channels below high head spillways on rock foundations. *Hydrotechnical Construction*, 9, 917-922, (1978).